



Granite Particle Flow Modeling Method Based on Digital Image Processing and Mesoscopic Parameter Calibration

Jin Pi, Jun Feng, Ke Li*, Heyi Liu, Jiangrong pei, Tiannan Chen, Yu Li

China Institute of Water Resources and Hydropower Research, Beijing 100048, China

*Corresponding author E-mail: like052100@163.com

Abstract. The transportation and civil construction sectors have placed higher demands on the study of the stability and mechanical behavior of geotechnical materials. In particular, the precise simulation of the microstructure of rock masses is critical for engineering design and safety assessments in tunnels and underground projects. To address the challenges of accurately reproducing the internal compositional differences and mesoscopic structures of rock-like materials in particle flow modeling, digital image processing technology was employed to develop a refined PFC simulation model for granite standard specimens, and mesoscopic parameters for parallel bond contacts were also calibrated. The results show that digital image processing effectively extracts the boundaries between different mineral components, such as quartz, feldspar, and mica, restoring the complex internal geometric structure of granite. The mesoscopic parameters significantly influencing the macroscopic deformation behavior of the model are the contact modulus and the normal-to-shear stiffness ratio. Parameters affecting the macroscopic load-bearing capacity include the friction coefficient, tensile strength, cohesion, and internal friction angle. Based on the final calibrated mesoscopic parameters, the PFC simulation model demonstrates good agreement with the experimental results of the granite standard specimens under uniaxial compression, indicating that the calibration method for mesoscopic parameters is both reasonable and effective.

Keywords: Digital image processing; PFC; Mesoscopic parameter; Granite; Uniaxial compression test

1 Introduction

In transportation infrastructure and civil construction projects, the design and construction of underground structures such as tunnels, underground garages, and subway stations impose stringent requirements on the study of rock mass stability. The design of underground structures must account for complex geological conditions and the heterogeneity of rock masses, which directly determine the long-term stability and safety of these structures. Consequently, in projects involving tunnel excavation and underground space development, studying the micromechanical properties of rock masses and their influence on macroscopic behavior has become a focal point for both

academia and the engineering industry. With the advancement of computer technology, numerical simulation techniques [1] have been increasingly applied to the study of failure mechanisms in hard and brittle rocks, in which the discrete element method (DEM) offers distinct advantages over other numerical simulation methods. The particle flow code (PFC) method [2][3], based on discontinuous medium theory, models materials as a collection of rigid particles, and by simulating the fluid-like motion of particles under external or internal forces, PFC connects the mesoscopic mechanics of particles with the macroscopic mechanical properties of rocks. The interactions between particles are used to reflect the macroscopic mechanical behavior of materials, thereby providing a mesoscopic explanation for macroscopic phenomena, which makes PFC inherently advantageous for simulating the failure behavior of heterogeneous materials. At present, it has become a powerful tool for investigating the fundamental characteristics of rock-like materials, their mechanical responses under various stress paths, and the development of fractures.

However, natural rock materials are heterogeneous and discontinuous, typically composed of various mineral constituents with significant differences in their physical and mechanical properties [4][5] and failure characteristics under load. Moreover, rocks often contain a multitude of random and complex mesoscopic structures, which greatly influence their ultimate failure modes. Current approaches to simulate these compositional differences and mesoscopic structures often rely on statistical analysis to generate particle groups using regular shapes such as rectangles, circles, triangles, or ellipses [6][7]. These methods are not only time-consuming and cumbersome, creating practical challenges, but also fail to capture the intricate geometric shapes of actual rock interiors. Furthermore, there is limited research demonstrating the extent to which these particle grouping methods accurately represent the true heterogeneity of rock materials, making it difficult to obtain realistic mechanical properties of rock-like materials.

In recent years, with the continuous progress of digital image processing technology [8][9], researchers began to use digital image technology to analyze the fundamental characteristics of rock materials with different mineral compositions, and try to combine it with numerical simulation technology, and some results have been achieved. Building on this, to address the challenge of reproducing the compositional differences and mesoscopic structures of rock materials in particle flow mesoscopic simulation models, this study utilized digital image processing technology and the PFC^{2D} software to construct a particle flow numerical simulation model of granite composed of three mineral components and calibrated the mesoscopic parameters [10][11]. The findings of this study provide a valuable reference for the precise simulation and analysis of rock material mesoscopic behavior in numerical models.

2 Mesoscopic Simulation Modelling Method of Granite Based on Digital Image Processing

Digital image processing involves converting image information into digital data for computer-based processing. Images consist of a series of pixels arranged in a rectangular grid, with each pixel representing information such as color and brightness. Based

on differences in color and grayscale, images can be categorized into four types: RGB color images, binary images, grayscale images, and indexed images. Grayscale images differentiate materials based on the brightness of their components, with pixel brightness represented by an integer called the grayscale value. Digital images, composed of matrices of pixels with varying grayscale values, can be used to generate particle flow simulation models. The specific steps for this process are as follows:

(1): Convert the colored digital image of granite into a grayscale image.

(2): Extract the grayscale gradient of each pixel in the grayscale image. Using the characteristic that the gradient at the edges of pixels is slightly greater than within the interior, identify the boundaries between different materials.

(3): Perform binary image processing on the identified boundaries by setting the pixels outside the boundary to 1 and the remaining pixels to 0.

(4): After generating the boundary for two materials, repeat the binary image processing steps to generate boundaries for additional materials until all materials are distinguishable.

In this study, the surface image of granite blocks from the Kashgar region in Xinjiang were selected for digital image processing, and the real-color digital image of the granite is shown in Figure 1(a). The image dimensions were 50 mm × 100 mm, and denoising was applied prior to model generation to improve clarity. The primary mineral components of the granite block include quartz, mica, and feldspar, with distinct differences in color among the minerals evident in the image.

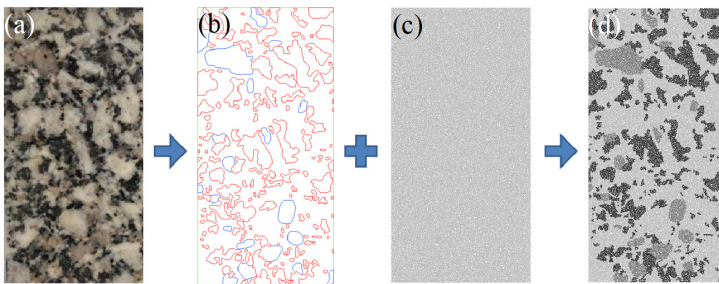


Fig. 1. Cylindrical standard specimens of granite

Through digital image processing, the boundaries between different mineral components of granite block can be extracted (Figure 1(b)). After establishing uniformly distributed circular particles with radius ranging from 0.2 mm to 0.35 mm and density of 2600 kg/m³ (Figure 1(c)), the extracted boundaries are then imported into the particles, and particles of different components are grouped according to the boundaries. This process results in the PFC simulation model of the granite standard specimen shown in Figure 1(d). In Figure 1(d), the colors transition from dark to light, representing mica, feldspar, and quartz, respectively. The model contains a total of 17,424 particles, including 11,160 quartz particles, 1,621 feldspar particles, and 4,643 mica particles, and the parallel bond contact model, which is suitable for simulating the mechanical properties of rock-like materials, is used for the interactions between particles.

3 Parameter Calibration in PFC

The predictive accuracy of particle flow code (PFC) simulations fundamentally relies on appropriate selection of contact parameters at the microscale. These particle-scale interactions collectively govern the emergent macroscopic behavior of modeled rock materials. Current calibration challenges arise from three inherent complexities: (1) the coupled nature of multiple micro-parameters, (2) absence of direct analytical relationships between particle-scale properties and bulk mechanical responses, and (3) requirement for empirical parameter optimization through computational-experimental comparisons. To address these challenges, this study implements a systematic parameterization strategy combining quantitative analysis with controlled variable testing. Initial reference values from Table 1 serve as baseline inputs for the parallel bond model, which simulates interparticle cementation through six key parameters: contact modulus, stiffness anisotropy ratio (normal-to-shear), frictional resistance, bond tensile strength, cohesive strength, and internal friction characteristics. Through sequential modification of individual parameters while maintaining others constant, we establish parametric sensitivity correlations by comparing numerical simulation outputs with laboratory-derived granite properties under uniaxial compression. This methodology enables precise identification of how specific microscale interactions influence macroscopic phenomena including stress-strain behavior, peak strength development, and fracture propagation patterns.

Table 1. Initial mesoscopic parameters of the parallel bond model

Mesoscopic parameter	Initial value	Range of values				
Contact modulus/GPa	45	10	30	45	60	80
Normal-to-shear stiffness ratio k_n/k_s	2.75	1	2	2.75	3.25	3.75
Coefficient of friction	0.5	0.1	0.3	0.5	1	1.5
Tensile strength/MPa	9	1	5	9	19	29
Cohesion /MPa	43	23	33	43	53	63
Internal friction angle/ $^{\circ}$	30	10	20	30	40	50

3.1 Influence of Contact Modulus on Macroscopic Mechanical Properties

According to previous studies, the overall elastic modulus of the PFC simulation model is most strongly correlated with the contact modulus of the particles. Figure 2 presents the stress-strain curves for PFC simulation models with varying contact modulus.

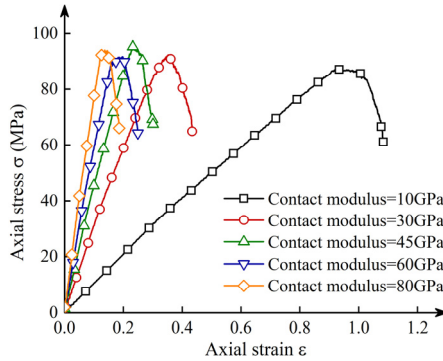


Fig. 2. Stress-strain curves corresponding to different contact modulus

The analysis reveals that increasing the contact modulus leads to a noticeable steepening of the elastic phase slope in the stress-strain relationship, accompanied by a consistent reduction in strain at peak strength. This trend suggests that higher contact moduli substantially enhance the model's effective elastic modulus while diminishing its capacity to undergo deformation. Although a marginal decrease in peak strength (approximately 90 MPa) is recorded at 10 GPa contact modulus, subsequent modulus values demonstrate stable peak strengths clustering around this threshold. Consequently, the contact modulus parameter exhibits minimal influence on the model's ultimate load-bearing characteristics.

3.2 Influence of k_n/k_s on Macroscopic Mechanical Properties

Within the computational framework of the parallel bond contact model, the contact modulus is governed by both normal and shear stiffness parameters. Altering the ratio of normal to shear stiffness significantly impacts the macroscopic stress-strain response of the material. As illustrated in Figure 3, PFC simulations reveal distinct stress-strain relationships under varying normal-to-shear stiffness ratios, demonstrating the critical role of this parameter in modeling mechanical behavior.

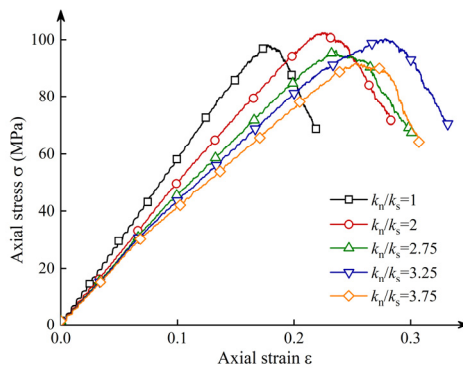


Fig. 3. Stress-strain curves corresponding to different k_n/k_s

As illustrated in Figure 3, the elastic phase slope of the stress-strain curve diminishes progressively with higher stiffness ratios, demonstrating a corresponding reduction in the macroscopic elastic modulus. Notably, the strain at peak strength exhibits an initial positive correlation with the stiffness ratio. However, a notable reversal occurs beyond a critical threshold of 3.75, suggesting that while the normal-to-shear stiffness ratio can amplify macroscopic deformation capacity within a limited range (below 3.25), excessive values may compromise this behavior. Further analysis reveals no statistically significant correlation between the overall peak strength and stiffness ratio variations, as the measured values oscillate consistently between 90 and 100 MPa. This observation confirms that the normal-to-shear stiffness ratio exerts minimal influence on the macroscopic load-bearing capacity of the system.

3.3 Influence of Coefficient of Friction on Macroscopic Mechanical Properties

The coefficient of friction is a mesoscopic parameter directly assigned to particles. Figure 4 records the stress-strain curves of PFC simulation models with varying friction coefficients.

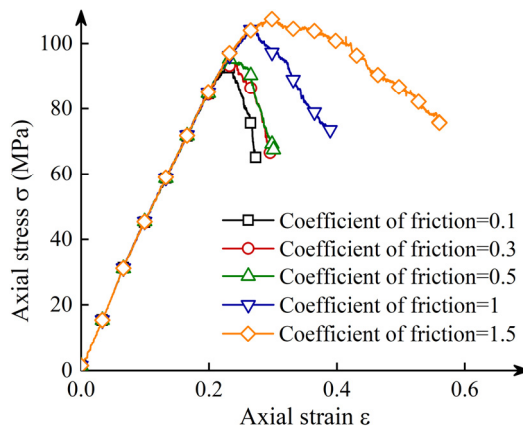


Fig. 4. Stress-strain curves corresponding to different coefficient of friction

It can be observed that the elastic stages of the stress-strain curves corresponding to different friction coefficients nearly overlap, indicating that this parameter has no significant effect on macroscopic deformation behavior. However, the overall peak strength increases with the friction coefficient, rising from 93.2 MPa at a friction coefficient of 0.1 to 106.1 MPa at a friction coefficient of 1.5, with an increase of approximately 13.84%. This is because higher friction coefficients result in rougher contact surfaces between particles, leading to greater frictional resistance during relative displacement. Consequently, the overall model, composed of particle assemblies, demonstrates a stronger ability to resist external loads. Additionally, as the friction coefficient increases, the post-peak phase of the curves becomes more gradual, showing a transition from brittle failure to ductile failure behavior.

3.4 Influence of Tensile Strength on Macroscopic Mechanical Properties

Tensile strength is a mesoscopic parameter in the parallel bond model associated with the normal force at contacts. Figure 5 illustrates the stress-strain curves of PFC simulation models with varying tensile strengths.

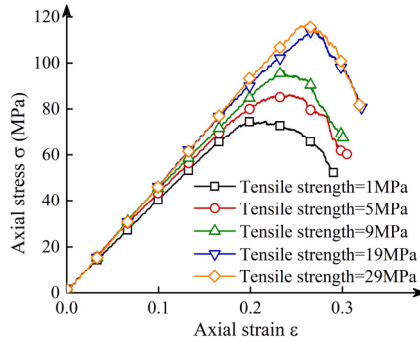


Fig. 5. Stress-strain curves corresponding to different tensile strength

From figure 5, as tensile strength increases from 1 MPa to 29 MPa, the model's overall peak strength rises from 73.2 MPa to 119.2 MPa, an increase of over 62.84%, which indicates that macroscopic load-bearing capacity is highly sensitive to changes in tensile strength. Furthermore, with the increase in tensile strength, the slope of the elastic stage of the stress-strain curves increases slightly, suggesting a marginal rise in the elastic modulus of the model. This implies that increasing tensile strength can slightly reduce macroscopic deformation capacity, although the effect is not particularly significant.

3.5 Influence of Cohesion on Macroscopic Mechanical Properties

Cohesion is a mesoscopic parameter in the parallel bond model associated with the tangential force at contacts. Figure 6 presents the stress-strain curves of PFC simulation models with varying cohesion values.

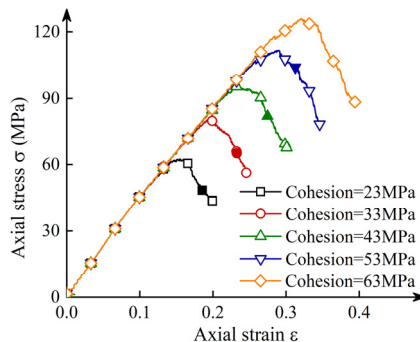
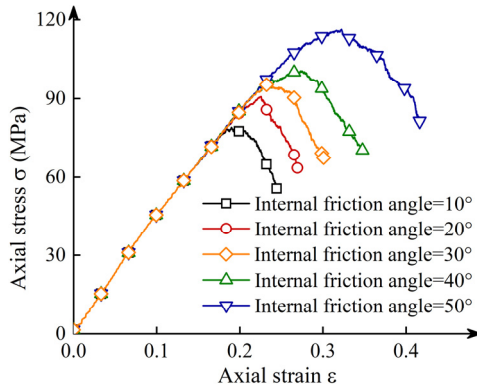


Fig. 6. Stress-strain curves corresponding to different cohesion

The figure demonstrates that as cohesion increases from 23 MPa to 63 MPa, the overall peak strength of the model rises from 63.3 MPa to 123.6 MPa, an increase of over 95.26%, which indicates that macroscopic load-bearing capacity is highly sensitive to changes in cohesion. Additionally, the shapes of the stress-strain curves for different cohesion values are essentially identical. The elastic segments of the curves almost overlap, and the post-peak slopes remain nearly constant, suggesting that this microscale parameter has virtually no influence on the macroscopic deformation behavior.

3.6 Influence of Internal Friction Angle on Macroscopic Mechanical Properties

Internal friction angles is another mesoscopic parameter in the parallel bond model associated with the tangential force at contacts. Figure 7 illustrates the stress-strain curves of PFC simulation models with varying internal friction angles.

**Fig. 7.** Stress-strain curves corresponding to different internal friction angle

As the internal friction angle increases from 10° to 50° , the overall peak strength of the model rises from 78.1 MPa to 113.7 MPa, an increase of over 45.58%, which indicates that the internal friction angle is also a sensitive factor affecting macroscopic load-bearing capacity. The elastic segments of the stress-strain curves for different internal friction angles are nearly identical. However, the slopes of the post-peak segments gradually decrease as the internal friction angle increases, indicating a transition in the overall failure mode from brittle failure to ductile failure. This is because, after the peak strength is reached and fractures begin to interconnect, the load-bearing and deformation capabilities of the model are primarily determined by the frictional forces between particles. Therefore, models with larger internal friction angles exhibit relatively higher post-peak load-bearing and deformation capabilities.

3.7 Results of Mesoscopic Parameter Calibration and Validation

Based on the influence of mesoscopic parameters on the macroscopic mechanical properties of the model, the calibration process first modifies the parameters that significantly affect the macroscopic properties. The numerical results are then compared with the physical model test results. Once the model's macroscopic properties fall within the appropriate range, the next parameter is adjusted. Since the granite block modeled in this study consists of three mineral components—quartz, feldspar, and mica—different mesoscopic parameters are assigned to each mineral component. To simplify the calibration process, the mineral components are distinguished primarily by mesoscopic parameters related to parallel bond contact between particles, while parameters such as contact modulus, stiffness ratio, and coefficient of friction are set to the same values. The final calibrated mesoscopic parameters for the three mineral components are shown in Table 2. Based on Table 2, the PFC simulation model and the granite standard specimen's experimental results under the uniaxial compression stress path are shown in Table 3.

Table 2. Mesoscopic parameters of the three mineral components

Materials	Contact modulus (GPa)	Normal-to-shear stiffness ratio k_n/k_s	Coefficient of friction	Tensile strength (MPa)	Cohesion (MPa)	Internal friction Angle (°)
Quartz	19	1.9	1	80	95	70
Feldspar	19	1.9	1	65	75	60
Mica	19	1.9	1	45	55	50

Table 3. Comparison of the uniaxial compression test results between the PFC simulation model and the granite standard specimen

Name of test	Peak strength (MPa)	Elastic modulus (GPa)	Poisson's ratio
Granite standard specimen test	107.4	18.7	0.17
PFC simulation model test	104.9	16.5	0.18

It can be seen that the peak strength of the PFC simulation model differs from the granite standard specimen by 2.33%, the elastic modulus differs by 11.76%, and the Poisson's ratio differs by 5.88%. Overall, the results of the uniaxial compression test of the PFC simulation model are in good agreement with those of the granite standard specimen, indicating that the calibration method for this set of mesoscopic parameters is reasonable and effective.

4 Conclusion

In this study, digital image processing technology was used to develop a refined PFC simulation model for the granite standard specimen. By comparing the PFC model with the experimental results of the granite standard specimen under uniaxial compression

stress, the mesoscopic parameters of the parallel bond contact model were calibrated. The following conclusions were drawn:

1. Digital image processing can extract the boundaries between different mineral components, such as quartz, feldspar, and mica. By using these extracted boundaries for particle grouping, the complex geometric structure of granite can be accurately restored.

2. The mesoscopic parameters that have a significant impact on the model's macroscopic deformation ability are the contact modulus and normal-to-shear stiffness ratio. Increasing the contact modulus significantly enhances the model's macroscopic elastic modulus, but the effect on the bearing capacity is minimal. Increasing the normal-to-shear stiffness ratio can improve macroscopic deformation ability within a certain range, but the value should not exceed 3.25.

3. The macroscopic bearing capacity of the model is governed by four key mesoscopic parameters: friction coefficient, tensile strength, cohesion, and internal friction angle. Experimental data reveal distinct enhancement patterns for each parameter. Specifically, increasing the friction coefficient from 0.1 to 1.5 enhances the bearing capacity by approximately 13.84%, with values rising from 93.2 MPa to 106.1 MPa. A more pronounced effect is observed in tensile strength, where elevating this parameter from 1 MPa to 29 MPa results in a substantial 62.84% improvement, boosting capacity from 73.2 MPa to 119.2 MPa. Cohesion demonstrates the most significant influence, as raising it from 23 MPa to 63 MPa nearly doubles the bearing capacity (95.26% increase), escalating from 63.3 MPa to 123.6 MPa. Similarly, expanding the internal friction angle from 10° to 50° yields a 45.58% enhancement, with capacity values progressing from 78.1 MPa to 113.7 MPa. These quantitative relationships collectively demonstrate the critical role of mesoscale material properties in determining structural performance at the macroscopic level.

4. Based on the final calibrated mesoscopic parameters, the PFC simulation model's peak strength differs from the granite standard specimen by 2.33%, elastic modulus by 11.76%, and Poisson's ratio by 5.88%. The uniaxial compression test results of both are in good agreement, indicating that the calibration of this set of mesoscopic parameters is reasonable and effective.

Acknowledgments

This work was financially supported by grants from the National Natural Science Foundation of China (Grant Nos. 52179121), IWHR Research & Development Support Program (Grant No. GE0145B012021), and Science and Technology Project of State Grid Corporation of China (Grant No. 5200-202455105A-1-1-ZN)

References

1. Xu H R, Liu P, Liu Q S, Cao X, Huang X, Luo X and Deng P H 2024 Numerical simulation on direct tensile behavior of rock materials using FDEM *J. Journal of Central South University (Science and Technology)* **55** 3416-3425

2. Liu H Y, Liu L P, Wang X G, Pei J R and Chen T N 2024 Research on the macroscopic and microscopic failure mechanisms and damage deterioration patterns of granite under unloading paths *J. International Journal of Geomechanics* **24** 9856
3. Liu J, Cong Y, Zhang L M and Wang Z Q 2021 Mesoscopic damage mechanism of granite under true triaxial loading and unloading *J. Journal of Central South University (Science and Technology)* **52** 2677-2688
4. Gong H L, Luo Y, Xu K, Wang X Y, Tao Y H and Li X P 2023 Mechanical characteristics of failure and rockburst proneness of fractured granite from Shuangjiangkou hydropower station under triaxial loading and unloading *J. Bulletin of Engineering Geology and the Environment* **82** 256
5. Du K, Li X F, Yang C Z, Zhou J, Chen S J and Manoj K 2020 Experimental investigations on mechanical performance of rocks under fatigue loads and biaxial confinements *J. Journal of Central South University* **27** 2985-2998
6. Liu H M, Ni C Y, Wang X H, Wang M Q, Ma X Q, Cao L and Wang Y G 2024 Particle flow analysis of crack propagation characteristics of cross jointed rock under uniaxial compression *J. Chinese Journal of Rock Mechanics and Engineering* **43** 3710-3721
7. Duan K, Jiang R H, Li X J, Wang L C and Yang Z Y. 2023 Examining the influence of the loading path on the cracking characteristics of a pre-fractured rock specimen with discrete element method simulation *J. Journal of Zhejiang University-SCIENCE A* **24** 332-350
8. Tang Y, He L, Lu W, Huang X, Wei H and Xiao H G 2021 A Novel approach for fracture skeleton extraction from rock surface images *J. International Journal of Rock Mechanics and Mining Sciences* **142** 104732
9. Bu J W, Chen X D, Hu L P, Yang H Q and Liu S S 2020 Experimental study on crack propagation of concrete under various loading rates with digital image correlation method *J. International Journal of Concrete Structures and Materials* **14** 1-20
10. Zhang X P and Wong Y N L 2012 Cracking processes in rock-like material containing a single flaw under uniaxial compression: a numerical study based on parallel bonded-particle model approach *J. Rock Mechanics and Rock Engineering* **45** 711-737
11. Xiao F K, Xie K, Gu Y, Liu G and Hao C B 2024 Mesoscopic parameter calibration method for collapsed body considering phase states-using parallel bonding model as an illustration *J. Rock and Soil Mechanics* **45** 13-24

Open Access This chapter is licensed under the terms of the Creative Commons Attribution-NonCommercial 4.0 International License (<http://creativecommons.org/licenses/by-nc/4.0/>), which permits any noncommercial use, sharing, adaptation, distribution and reproduction in any medium or format, as long as you give appropriate credit to the original author(s) and the source, provide a link to the Creative Commons license and indicate if changes were made.

The images or other third party material in this chapter are included in the chapter's Creative Commons license, unless indicated otherwise in a credit line to the material. If material is not included in the chapter's Creative Commons license and your intended use is not permitted by statutory regulation or exceeds the permitted use, you will need to obtain permission directly from the copyright holder.

